



# Measurements of evapotranspiration from eddy-covariance systems and large aperture scintillometers in the Hai River Basin, China

S.M. Liu<sup>\*</sup>, Z.W. Xu, Z.L. Zhu, Z.Z. Jia, M.J. Zhu

State Key Laboratory of Remote Sensing Science, School of Geography, Beijing Normal University, Beijing 100875, China

## ARTICLE INFO

### Article history:

Received 27 July 2012

Received in revised form 18 November 2012

Accepted 9 February 2013

Available online 26 February 2013

This manuscript was handled by

Konstantine P. Georgakakos, Editor-in-Chief,

with the assistance of Venkat Lakshmi,

Associate Editor

### Keywords:

Evapotranspiration

Eddy covariance system

Large aperture scintillometer

Hai River Basin

## SUMMARY

Evapotranspiration (ET) observations were made for 3 years (2008–2010), using eddy covariance (EC) systems and large aperture scintillometers (LAS), in typical underlying surfaces across the Hai River Basin: orchards (Miyun, MY), cropland in the suburbs (Daxing, DX), and cropland in the plains (Guantao, GT). Reliable data were obtained after carefully data processing, and the seasonal and interannual variability in ET was quantitatively analyzed. The annual ET during 2008–2010 ranged from 510–730 mm for the EC measurements and 430–560 mm for the LAS measurements. The differences in ET among the years and sites were connected with differences in soil moisture and crop growing conditions. The difference in the source areas of EC and LAS measurements and the heterogeneity in their source areas are the primary causes of the discrepancy between EC and LAS measurements. The EC and LAS measurements are compared to the field water balance method calculation and MOD16 ET (the MODIS ET product from the MODIS Global Evapotranspiration Project), respectively. The average difference was 0.85% (mean relative error) and 33.80 mm (root mean square error) between the EC measurements and field water balance method calculations, and 7.72% and 47.08 mm between LAS measurements and MOD16 ET from 2008 to 2010 at the three sites. We found a decreasing tendency for ET in the past 15 years across the Hai River Basin, especially after the year of 2005.

© 2013 Elsevier B.V. All rights reserved.

## 1. Introduction

Evapotranspiration (ET) is an important parameter in the interactions between soil, vegetation, and the atmosphere, and it is a central part of surface energy and water budgets. Many ecosystem parameters and processes, such as soil moisture content, vegetation productivity, ecosystem nutrients, and water budgets, are all influenced by ET (Wever et al., 2002). On a global scale, approximately 64% of precipitation over land returns to the atmosphere through ET (Rivas and Caselles, 2004). The quantitative analysis of ET is an essential strategy for the study of the global climate change and watershed resources management. Therefore, it is very important to study the characteristics of the variation in ET over different land covers.

The Hai River Basin (HRB) is located between 112.0° to 119.8°E and 35.0° to 42.8°N and covers 318,200 km<sup>2</sup> in northern China, accounting for 3.3% of China's total land area. The average annual water resources in the HRB only account for 1.5% of the national total but supply water to 10% of the population of the country,

including Beijing, Tianjin, and other large cities. The average annual water resources (1956–1998) of the HRB are 372 billion m<sup>3</sup>, but the per capita availability is only 250–300 m<sup>3</sup>/year (Wang et al., 2011), 1/7 of the national average for China and 1/24 of the global average (Xia et al., 2006). The HRB is also one of the major food production areas in China; however, due to the over-exploitation, the groundwater table in the alluvial plain is declining (Liu et al., 2001), which has become the leading threat to the agricultural production. In the HRB, the primary water use is consumption by agriculture, utilizing 67% of the total (irrigation amount); this proportion reaches 80% if other agricultural water uses are included (Liu et al., 2005). Therefore, methods for improving agricultural water use efficiency are an important subject for study. To achieve the goal of “agricultural water saving”, it is particularly important to clarify the variation in ET among different underlying surfaces in the HRB.

Currently, the general equipment used to measure ET includes the lysimeter, Bowen-ratio energy balance system, eddy covariance system (EC), and scintillometers, etc. Among these equipments, the EC and scintillometers are widely used around the world. The EC can directly measure the water vapor, heat and carbon dioxide flux, and it is considered as the standard method for measuring water vapor and heat fluxes (Aubinet et al., 2000; Baldocchi, 2003). The measurement scale of EC is generally hundred meters (Jia et al., 2012). Wilson and Baldocchi

<sup>\*</sup> Corresponding author. Address: State Key Laboratory of Remote Sensing Science, School of Geography, Beijing Normal University, No. 19 Xijiekouwai Street, Beijing 100875, China. Tel.: +86 10 58802240; fax: +86 10 58805274.

E-mail address: [smliu@bnu.edu.cn](mailto:smliu@bnu.edu.cn) (S.M. Liu).

(2000) studied the surface energy balance components of a broad-leaved deciduous forest in North America using 3 years of EC data, especially the ET characteristics and its controlling factors in the forest ecosystem; Wever et al. (2002) investigated the seasonal and interannual variation in ET and its controlling factors in the grassland ecosystem using three plant growing seasons of EC data; Suyker and Verma (2009) discussed the variation in ET in irrigated and rainfed croplands using EC data from 5 consecutive years, comparing the ET associated with different land covers and soil moisture and calculating the water use efficiency. These findings revealed the quantitative variations in ET in different study areas and provided the abundant information for the relevant department decision-makers and the subsequent researchers. Nevertheless, the EC method has limitations, such as data processing and quality control methods under complex conditions (e.g., unfavorable weather and topography) and the problem of surface energy imbalance in EC observations (Hammerle et al., 2007; Mauder et al., 2007a; Foken et al., 2010).

In the early 1990s, an increasing number of researchers focused on studying the large-scale (kilometers scale) ET, and the scintillometer technique was adapted for this purpose. Since the late 1990s, the large aperture scintillometer (LAS) has been successfully used in many field experiments over homogeneous and heterogeneous surfaces (e.g., Flevoland, LITFASS-1998, LITFASS-2003). The LAS can measure the sensible heat flux, and the kilometer-scaled ET can be acquired by combining the available energy (net radiation minus surface soil heat flux) (Meijninger et al., 2002a). Beyrich et al. (2002) studied the seasonal variation of sensible heat flux under mixed forest and cropland surfaces using more than one year of LAS observation data (LITFASS-1998 experiment, Germany), and compared it with the results of a numerical weather prediction model, which showed consistent results. Hemakumara et al. (2003) investigated the characteristics of the variation in ET derived from LAS over heterogeneous surfaces using ten months of observation data collected in the southeast of Colombo, Sri Lanka, and validated the surface energy balance algorithm for land (SEBAL) model. Schüttemeyer et al. (2006) discussed the diurnal variations in latent heat and sensible heat flux measured by LAS over two types of underlying surfaces (mixed surfaces with orchards and shrubs, sparse grass) in Ghana and found that the LAS appeared to perform more realistically than the EC method in drying semi-arid terrain. Ezzahar et al. (2007) studied the seasonal variation in latent and sensible heat flux over heterogeneous surfaces (sparsely irrigated olive yards) using more than one year of LAS observation data in Morocco and compared the results with the EC measurements, which showed that LAS measurements can be reliably predicted at a large scale. Liu et al. (2011) investigated the seasonal variation in sensible heat flux across the Heihe River Basin as measured by EC and LAS and found the causes of the differences between two, namely, the energy imbalance of EC, the heterogeneity of the underlying surfaces, and the different source areas of LAS and EC measurements. At present, the primary application of LAS observation data is, to validate remote sensing models (Hemakumara et al., 2003; Kleissl et al., 2009) and to compare these data with other measurements at different scales (Hoedjes et al., 2007; Von Randow et al., 2008). The LAS also has its limitations, such as meteorological limitations in long-term operations (including issues with precipitation, poor visibility, and weak turbulence), and methodological limitations (such as signal saturation and the inner-scale dependence of the signal), and tower vibrations (Moene et al., 2009). Thus, data processing of EC and LAS must be performed carefully when analyzed the characteristics of the variation in ET, especially under complex conditions (Meijninger et al., 2002a).

In the HRB, most of the flux measurement instruments used are lysimeters (Liu et al., 2002; Liu and Luo, 2010), with only a few

studies using EC for the long-term ET analysis (Lei and Yang, 2010), and there have been no publications on long-term ET analysis measured by LAS up to now (additionally, few such reports have been published worldwide). Based on three years (2008–2010) of EC and LAS data for the HRB, the following issues were studied: (i) Quality assessment of EC and LAS data, (ii) Analysis of the source areas of EC and LAS over different underlying surfaces, (iii) Analysis of the seasonal and interannual variations in ET by EC and LAS over different underlying surfaces, and (iv) Comparison of the EC and LAS measurements with the results of the field water balance calculation method and a remote sensing model, respectively, and comparative analysis with the findings obtained by other researchers for the basin. The primary objective of this paper is to improve the quantitative understanding of ET variation over the HRB.

## 2. Materials and methods

### 2.1. Site description and measurements

Three sites in the HRB were selected, namely, the Miyun (MY), Daxing (DX) and Guantao (GT) sites, located in the northern (MY, 40°37'50.82"N, 117°19'23.83"E), middle (DX, 39°37'16.7"N, 116°25'37.2"E) and southern parts (GT, 36°30'54.1"N, 115°07'38.7"E) of the basin, representing three typical underlying surfaces: northern mountains (orchards, maize), cropland in the central suburbs (winter wheat/maize, vegetables), and cropland in the southern plains (winter wheat/maize, cotton). MY is located in a valley oriented in a northeast–southwest direction, with a town on the northwest side. The terrain around MY is somewhat rolling with a decline from the northeast to the southwest. The LAS transmitter and receiver were installed on two opposite hills along the valley, and the EC system was installed in an orchard 900 m from the LAS receiver. Both DX and GT are located in croplands with very flat terrain. At DX, the LAS transmitter and receiver were installed on two opposite towers in the southwest to northeast direction, and the EC system was installed in the transmitter side of the LAS. At GT, the LAS transmitter and receiver were installed on two towers in a north to south direction, with the EC system in the center of the optical path of the LAS. The specific locations of the sites are shown in Fig. 1.

### 2.2. Instrument

The instruments at each of the three sites included one eddy-covariance system (EC), one large aperture scintillometer (LAS), and one automatic weather station (AWS). The EC system has a 3D sonic anemometer (CSAT3, Campbell Scientific Inc., USA) measuring three-dimensional velocity and temperature and an open path infrared CO<sub>2</sub>/H<sub>2</sub>O gas analyzer (Li-7500, Li-Cor, USA) measuring CO<sub>2</sub> and H<sub>2</sub>O density. The data were stored in a CR5000 data logger (Campbell Scientific Inc., USA) at a sampling frequency of 10 Hz. The installation heights of the EC were 26.66 m, 3 m and 15.6 m at MY, DX and GT, respectively. All of the LASs are produced by Kipp & Zonen, Netherlands, the effective heights and path lengths were 35.86 m and 2420 m at MY, 29.6 m and 2480 m at DX, and 15.6 m and 2760 m at GT, respectively. The data logger for the LAS was a CR1000 unit (Campbell Scientific Inc., USA) operating at a sampling frequency of 1 Hz. The EC and LAS data were processed with an averaging time of 30 min. The AWS at each site obtained data on precipitation, wind speed/direction, air temperature/humidity, air pressure, radiation, soil temperature/moisture profile, surface infrared temperature, and soil heat flux. All of the AWS data were collected once each 10 s and the output data were stored at 10 min intervals. The data loggers used were CR10X

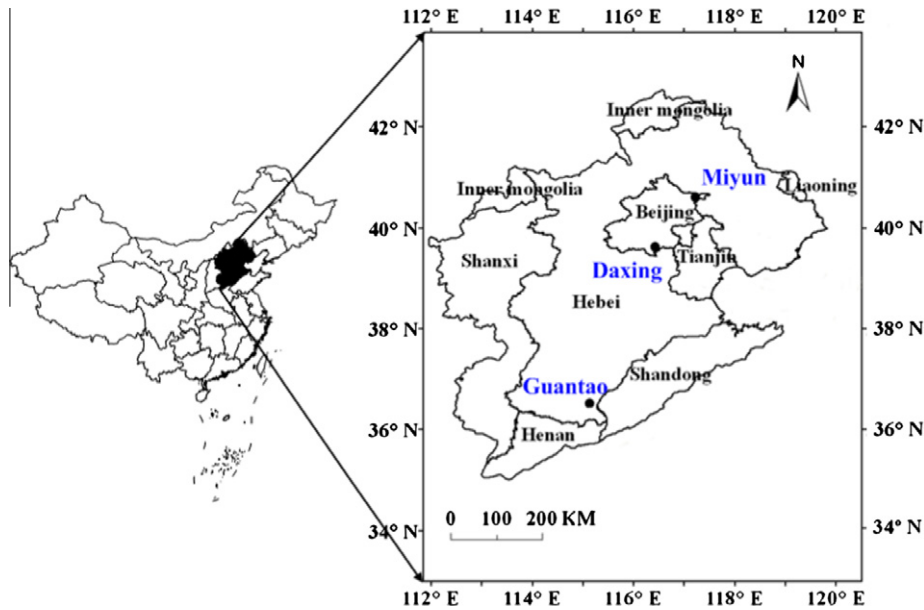


Fig. 1. The locations of the three study sites over the HRB.

Table 1

The observation instrument at the three sites.

Observed items	Sensor type
Sensible heat and latent heat flux	Li7500 and CSAT3, Li-cor
Height (m), MY: 26.66, DX: 3, GT: 15.6	and Campbell
Sensible heat flux	LAS, Kipp and Zonen
Height (m), MY: 35.86, DX: 27, GT: 15.6	
Path length (m), MY: 2420, DX: 2480, GT: 2760	
Air temperature/humidity	HMP45C, Vaisala
Height (m), MY: 10.66&30.56, DX: 10&27, GT: 4&12.5	
Wind speed/direction	03001, R.M. Young
Height (m), MY: 10.66&30.56, DX: 27, GT: 12.7	
Infrared temperature	IRTC-3, Avalon
Height (m), MY: 30.56, DX: 28, GT: 15.7	
Radiation	CNR1, Kipp and Zonen
Height (m), MY: 30.76, DX: 28, GT: 15.7	
Soil heat flux	HFT-3, Campbell (HFP01,
Depth (m), 0.02 at MY, DX and GT	Hukseflux at GT)
Soil temperature	AV-10T, Avalon
Nine depths at MY and GT: 0, 0.02, 0.05, 0.1, 0.2, 0.4, 0.6, 0.8, 1 m; eight depths at DX: 0.02, 0.05, 0.1, 0.2, 0.4, 0.6, 0.8, 1 m	
Soil moisture	ECH2O-10, Decagon
Seven depths at MY, DX and GT: 0.02, 0.05, 0.1, 0.2, 0.4, 0.6, 1 m	
precipitation	TE525, Campbell (52203, R.M. Young at MY)
Air pressure	CS100, Campbell (AV-410, Avalon at MY)
Landscape	MY: Orchard, Maize DX: winter wheat/maize, vegetable GT: winter wheat/maize, cotton
Maximum vegetation height (m)	MY: orchard (plum and apple tree): 4; maize: 2.2 DX: Maize: 2.2; winter wheat: 0.7; vegetable: 0.5 GT: maize: 2.2; winter wheat: 0.7; cotton: 1.2

### 2.3. Data processing

Data were processed rigorously using a uniform procedure at the three sites, which were measured using EC, LAS and AWS during the years of 2008 to 2010, as follows.

#### 2.3.1. Eddy covariance system

Raw data acquired at 10 Hz were processed using the post-processing software EdiRe (University of Edinburgh, <http://www.geo-s.ed.ac.uk/abs/research/micromet/EdiRe>), including spike removal, lag correction of H<sub>2</sub>O/CO<sub>2</sub> relative to the vertical wind component, sonic virtual temperature correction, the performance of the planar fit coordinate rotation, corrections for density fluctuation (WPL-correction), frequency response correction, etc. In addition to these processing steps, quality control of the half-hourly flux data was carried out in a four-step procedure: (i) data from periods of sensor malfunction were rejected (e.g., when there was a faulty diagnostic signal), (ii) data within 1 h before or after precipitation were rejected, (iii) incomplete 30 min data were rejected when the missing data constituted more than 3% of the 30 min raw record, and (iv) data were rejected at night when the friction velocity was below 0.1 m s<sup>-1</sup> (Blanken et al., 1998) (for GT 0.05 m s<sup>-1</sup>).

Because of the energy imbalance of EC, the water vapor and heat fluxes at the three sites may be underestimated, so the sensible and latent heat fluxes were corrected for closure on a daily basis using the Bowen ratio closure method (Twine et al., 2000). The corrected fluxes were only used to analyze the seasonal and inter-annual variations of ET at the three sites.

In long-term observations, missing data will occur due to instrument malfunction, poor maintenance, and bad weather conditions. The gap-filling methods of a look-up table (LUT) and mean diurnal variations (MDV) (Falge et al., 2001) were used to fill gaps in the flux measurement data. The LUT method was applied when the meteorological observation data were available synchronously; otherwise, the MDV method was used. The gap-filling data were used only to analyze the seasonal and interannual variations in ET.

#### 2.3.2. Large aperture scintillometer

The LAS is a device that derives the turbulent intensity through measuring the refractive index of air,  $C_n^2$  (m<sup>-2/3</sup>), which can be expressed as (Wang et al., 1978):

(Campbell Scientific Inc., USA, MY), DT85 (Datataker, DX), and CR1000 (Campbell Scientific Inc., USA, DX) units. Detailed descriptions are provided in Table 1.

$$C_n^2 = 1.12 \sigma_{\ln I}^2 D^{7/3} L^{-3} \quad (1)$$

where  $\sigma_{\ln I}^2$  is the variance of the natural logarithm of intensity fluctuations,  $D$  is the aperture diameter (m), and  $L$  is the path length (m).

Data were carefully screened to ensure the data quality of LAS, as follows: (i) data were rejected for  $C_n^2$  beyond the saturation criterion, which was determined according to Ochs and Wilson (1993); the upper limits of the  $C_n^2$  saturation were  $7.58 \times 10^{-14} \text{ m}^{-2/3}$ ,  $7.14 \times 10^{-14} \text{ m}^{-2/3}$ , and  $5.34 \times 10^{-14} \text{ m}^{-2/3}$  at MY, DX, and GT, respectively; (ii) data obtained during periods of precipitation were rejected; (iii) data were rejected when the demodulated signal was less than the threshold (MY:  $-30 \text{ mV}$ , DX and GT:  $-10 \text{ mV}$ ); (iv) data were rejected if collected at night during periods of weak turbulence; (v) data were rejected if collected when the sensor was malfunctioning.

Strictly speaking, temperature and humidity fluctuations cause fluctuations in the refractive index of air.  $C_n^2$  is therefore related to the temperature structure parameter  $C_T^2$  ( $\text{K}^2 \text{ m}^{-2/3}$ ), humidity  $C_q^2$  ( $\text{kg}^2 \text{ m}^{-6} \text{ m}^{-2/3}$ ), and the covariance term  $C_{Tq}$  ( $\text{K kg m}^{-3} \text{ m}^{-2/3}$ ). As a simplification, Wesely (1976) showed that for LAS, operating at a near-infrared wave length,  $C_n^2$  could be related to  $C_T^2$  by

$$C_T^2 = C_n^2 \left( \frac{T^2}{-7.87 \times 10^{-7} P} \right)^2 \left( 1 + \frac{0.03}{\beta} \right)^{-2} \quad (2)$$

where  $T$  is the air temperature (K),  $P$  is the air pressure (Pa), and  $\beta$  is the Bowen ratio. According to the Monin–Obukhov similarity theory (MOST), the sensible heat flux  $H_{LAS}$  ( $\text{W m}^{-2}$ ) can be calculated from the following equations:

$$\frac{C_T^2 (z_{LAS} - d)^{2/3}}{T_*^2} = f_T \left( \frac{z_{LAS} - d}{L_{Ob}} \right) \quad (3)$$

$$H_{LAS} = \rho_a C_p u_* T_* \quad (4)$$

$$u_* = \frac{k_v u}{\ln \left( \frac{z_u - d}{z_{0m}} \right) - \Psi_m \left( \frac{z_u - d}{L_{Ob}} \right) + \Psi_m \left( \frac{z_{0m}}{L_{Ob}} \right)} \quad (5)$$

where  $z_{LAS}$  is the effective height of the LAS (m), derived following the method proposed by Hartogensis et al. (2003), which is calculated from the scintillometer beam height along the path in conjunction with the weigh function of LAS (method 2 in his paper),  $d$  is the zero-plane displacement height (m), which is calculated from the simple relationship between  $d$  and the vegetation canopy height  $h_c$  (i.e.,  $d = \frac{2}{3} h_c$ ),  $L_{Ob}$  is the Obukhov length (m), and  $f_T$  is the stability function, defined as follows (Andreas, 1988). For unstable conditions (i.e.,  $L_{Ob} < 0$ ),  $f_T = 4.9 \left[ 1 - 6.1 \left( \frac{z_{LAS} - d}{L_{Ob}} \right) \right]^{-2/3}$ ; for stable conditions (i.e.,  $L_{Ob} > 0$ ),  $f_T = 4.9 \left[ 1 + 2.2 \left( \frac{z_{LAS} - d}{L_{Ob}} \right) \right]^{2/3}$ .  $C_p$  is the specific heat capacity of air at constant pressure ( $\text{J kg}^{-1} \text{ K}^{-1}$ ),  $\rho_a$  is the density of air ( $\text{kg m}^{-3}$ ),  $u_*$  is the friction velocity ( $\text{m s}^{-1}$ ),  $T_*$  is the temperature scale (K),  $k_v$  is the von Kármán constant (0.40),  $u$  is the wind speed ( $\text{m s}^{-1}$ ),  $z_u$  is the measurement height of the wind speed (m),  $z_{0m}$  is the aerodynamic roughness length (m), which is calculated with EC data based on the method suggested by Yang et al. (2003), which was obtained by minimizing a cost function assuming that the aerodynamic roughness length is constant over short periods of time (e.g., 10 days) and  $\Psi_m$  is the stability correction function for the momentum transfer (Paulson, 1970; Webb, 1970).

Because the scintillometer can only observe the intensity of atmosphere turbulence, it cannot determine the direction of the sensible heat flux. Thus, the difference in air temperature between two heights was used to judge the sign of the LAS flux at the three sites.

After the sensible heat was calculated, the latent heat flux (ET) could be estimated from the energy balance equation using the

measurements of net radiation and soil surface heat flux (Meijnnin-ger et al., 2002a).

$$LE_{LAS} = R_n - G_0 - H_{LAS} \quad (6)$$

where  $LE_{LAS}$  ( $\text{W m}^{-2}$ ) is the latent heat flux estimated by the LAS,  $R_n$  ( $\text{W m}^{-2}$ ) is the net radiation, and  $G_0$  ( $\text{W m}^{-2}$ ) is the soil surface heat flux to be calculated in Section 2.3.3.

A nonlinear regression method was used to fill the missing 30 min data for the periods of unstable conditions; for gaps occurring during the stable conditions, the gap was filled with zero and a dynamic linear regression method was used to fill in the missing daily data (Alavi et al., 2006). The gap-filling data were only used to analyze the seasonal and interannual variations in ET.

### 2.3.3. Automatic weather station

Observation items of the automatic weather station (AWS) are listed in Table 1. The data obviously beyond the range of physical possibility were rejected, and the gaps were filled by interpolation. Because the soil heat flux plates were buried at depths of 0.02 m in this study, the soil surface heat flux was estimated using the method proposed by Yang and Wang (2008), which is a temperature prediction–correction method based on the thermal exchange equation using the profile of soil temperature and moisture observations, as follows:

$$G_z = G(z_r) + \int_z^{z_r} \frac{\partial C_v T(z)}{\partial t} dz \quad (7)$$

where  $G_z$  is the soil heat flux ( $\text{W m}^{-2}$ ) at depth  $z$ ,  $t$  is the time (s),  $C_v$  is the soil heat capacity ( $\text{J kg}^{-1} \text{ K}^{-1}$ ),  $T$  is the soil temperature (K),  $z$  is the soil depth (m) (positive downward), and  $G(z_r)$  is the soil heat flux at reference depth  $z_r$ . In this study, the reference depth  $z_r$  was 1 m at the three sites. Therefore, we assumed that  $G(z_r) \approx 0$ .

Given the temperature profile  $T(z_i)$ , the soil surface heat flux,  $G_0$ , is:

$$G_0 = \frac{1}{\Delta t} \sum_{i=0}^{z_r} [c_v(z_i, t + \Delta t) T(z_i, t + \Delta t) - c_v(z_i, t) T(z_i, t)] \Delta z \quad (8)$$

where  $z_i$  is the depth of soil layer  $i$  (m),  $\Delta t$  is the time interval (s), and  $\Delta z$  is the thickness of a thin layer of the soil (m).

This method constructed the soil temperature profile and then corrected it using the measured soil temperature. By integrating Eq. (8), from the surface ( $z = 0$ ) to the reference depth ( $z_r = 1 \text{ m}$ ), one can obtain the soil surface heat flux.

### 2.3.4. Footprint model

Footprint analysis is now a recognized part of the establishment and the sitting of flux towers and the analysis of their output (Finnigan, 2004). The field of view of instruments (EC and LAS in this study) can be well defined by the so-called source area, the sizes and extent of which depend on many factors, such as the measurement height, atmospheric stability, wind speed and direction, surface roughness length, etc. Knowledge of the source areas of the EC and LAS measurements is clearly important before analyzing the characteristics of the energy and water vapor fluxes.

To estimate the flux footprint, the method proposed by Kormann and Meixner (2001), which is an Eulerian analytic flux footprint model, is implemented here to obtain the flux footprint of a single point vertical flux measurement  $f(x, y, z_m)$

$$f(x, y, z_m) = D_y(x, y) f^y(x, z_m) \quad (9)$$

where  $x$  is the downwind distance pointing against the average horizontal wind direction,  $y$  is the crosswind wind distance,  $z_m$  is the measurement height,  $f^y(x, z_m)$  is the crosswind integrated footprint, and  $D_y(x, y)$  is the Gaussian crosswind distribution function of the



lateral dispersion. It is worth noting that the observed wind velocity at  $z_m$  was used as an input item to gain the model parameters.

Combining the path-weighting function of the LAS (Meijninger et al., 2002b; Liu et al., 2011) with the above footprint model for point flux, we deduce the LAS flux observations,

$$f_{LAS}(x', y', z_m) = \int_{x_2}^{x_1} W(x) f(x - x', y - y', z_m) dx \quad (10)$$

where  $W(x)$  is the path-weighting function of the LAS,  $x_1$  and  $x_2$  are the locations of the LAS transmitter and receiver,  $x$  and  $y$  denote the points along the optical length of the LAS, and  $x'$  and  $y'$  are the coordinates upwind of each points  $(x, y)$ .

The monthly flux source area of the EC and LAS flux measurements was obtained as follows: (i) averaging every half-hourly footprint when the sensible heat fluxes were larger than zero, values dating from 22:00 to 6:00 BST (Beijing standard time) were also excluded; (ii) choosing an area of  $3 \text{ km} \times 3 \text{ km}$  with a 30 m resolution grid as an approximate area of the total source area around the measurement point for EC and the central part of the LAS optical path, respectively, the flux contribution of the chosen total source area was set at 80% for each month (50% for MY site).

### 3. Results and discussion

#### 3.1. Flux data quality

To ensure the accuracy of flux measurements, carefully data processing was applied (see Section 2.3). This section focuses on analyzing the quality of flux data collected by the EC and LAS.

##### 3.1.1. Eddy covariance system

The stationarity and integral turbulent characteristics test proposed by Foken and Wichura (1996) was used to assess each 30 min EC data collection. The data were divided into 9 classes using this test; classes 1–6 were available for general use, classes 7 and 8 were only for orientation (better than the gap filling procedure), and class 9 should be excluded (Foken et al., 2004). Meanwhile, to avoid the possible underestimation of flux data at night during periods of weak turbulence, these data were rejected using the friction velocity ( $u_*$ ) threshold method (Blanken et al., 1998) (MY and DX threshold were 0.1 m/s, GT was 0.05 m/s). In addition, data collected during system/logging failures, maintenance and calibration, or improper weather conditions were also rejected. The overall quality of data collected from 2008 to 2010 at the three sites is plotted in Fig. 2, which shows that the average available data percentage was approximately 84% at GT, 69% at MY, and

57% at DX during the three years. The observed EC flux data were adaptable for the long time series analyzed at the three sites, and the available data percentage was similar to results of the Fluxnet sites (the average data coverage during a year was 65%, Falge et al., 2001).

The power spectra (cospectra) were calculated using the fast Fourier transform (FFT) and Hanning filter method. Power spectra, showing the frequency contribution for three dimensions ( $u, v, w$ ), virtual temperature ( $T_v$ ), water vapor ( $\text{H}_2\text{O}$ ) and carbon dioxide ( $\text{CO}_2$ ) density, and cospectra ( $\text{WT}_v$ ,  $\text{WH}_2\text{O}$ ,  $\text{WCO}_2$ ) are shown in Fig. 3, where the  $x$ -axis is normal frequency ( $n, \text{Hz}$ ) and the  $y$ -axis is power spectra ( $S(n)$ ) or cospectra ( $\text{Co}_{wx}(n)$ ) multiplied by  $n$ . A typical day, 7 July 2009, was selected for this analysis. As expected, the spectra fall together in the inertial subrange, where they follow the  $-2/3$  slope quite well; the cospectra collapse in the inertial subrange, where they follow a slope close to  $-4/3$  (Fig. 3).

The energy balance ratio (EBR) is one of the main quality assessment methods for EC data (Aubinet et al., 2000). EBR was calculated using the EC data classes 1–8 at the three sites (Table 2) as follows:  $\text{EBR} = \frac{\sum (H + LE)}{\sum (R_n - G_0)}$ , where  $H$  and  $LE$  are the sensible heat and latent heat flux measured by EC, respectively. The EBR showed no obvious changes between different years within each site and fell within the range of 0.78–0.91, which is similar to values reported from other observations (Wilson et al., 2002; Oncley et al., 2007). The EBR in GT is best (the averaged value is 0.90), followed by DX (the averaged value is 0.83) and MY (the averaged value is 0.78). The cause of the imbalance is not clear; however, the primary reasons appeared to be unmeasured low-frequency contributions or secondary circulations due to the heterogeneity of the surface by EC measurements at a single station (Mauder et al., 2007b; Foken et al., 2010, 2011).

##### 3.1.2. Large aperture scintillometer

The theory of LAS measuring sensible heat flux was based on MOST; thus, the LAS data quality was usually judged by whether  $C_T^2$  from the LAS behaves according to MOST (Hoedjes et al., 2007). The observed values of  $C_T^2 (z_{LAS} - d)^{2/3} / T_*^2$  were plotted against  $(z_{LAS} - d) / L_{Ob}$  under unstable conditions for the entire data set (the sensible heat fluxes larger than  $50 \text{ W m}^{-2}$  were selected) in Fig. 4. The values of  $T_*$  and  $L_{Ob}$  were taken from the EC measurements together with the scaling curves described by De Bruin et al. (1993), Andreas (1988) and Thiermann and Grassl (1992).

As showed in Fig. 4, most of the measured values at GT followed the shape of the theoretical line, but for near-neutral conditions, the points were somewhat above the curve. Values at MY were

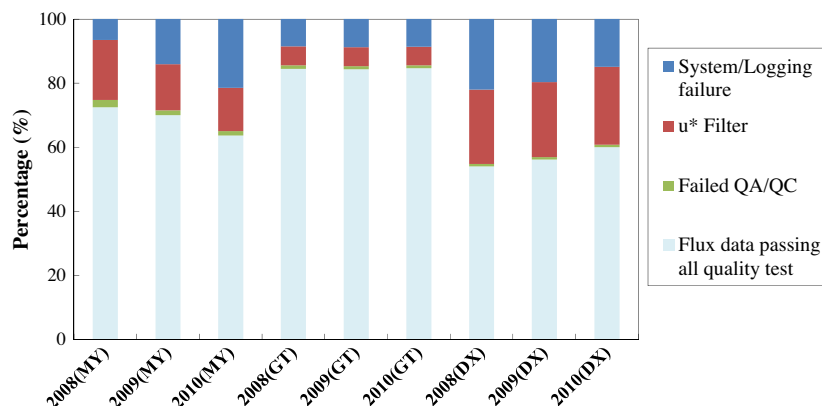


**Fig. 2.** The quality of the EC data during 2008–2010 at the three sites over the HRB (flux data passing all quality tests means the available data percentage. System/logging failure,  $u_*$  filter, and failed QA/QC means that data were missing or rejected during instrument maintenance and calibration, improper weather conditions, beyond the  $u_*$  threshold, and poor data at class 9, respectively).

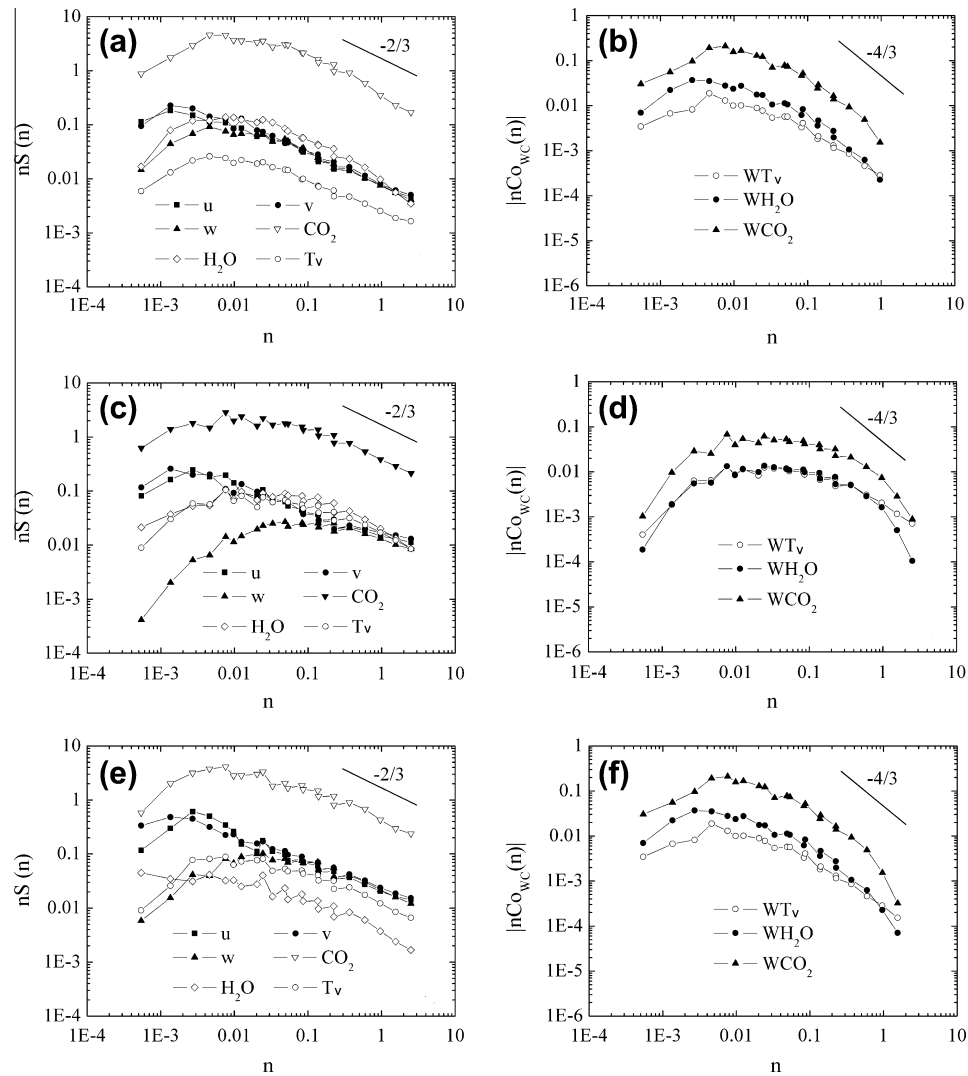


**Fig. 3.** Mean power spectra/cospectra (a, c, e are the power spectra for three dimensional velocity  $u$ ,  $v$ ,  $w$ ,  $\text{CO}_2$ ,  $\text{H}_2\text{O}$ , and  $T_v$  at MY, DX, GT, respectively; b, d, f are the cospectra for  $\text{WT}_v$ ,  $\text{WH}_2\text{O}$ ,  $\text{WCO}_2$  at MY, DX and GT, respectively) (data were the 8 half-hour periods from 10:00–14:00 on 7 July 2009).

**Table 2**

The energy balance ratio at the three sites.

Site	MY			DX			GT		
Year	2008	2009	2010	2008	2009	2010	2008	2009	2010
EBR	0.76	0.79	0.80	0.81	0.83	0.84	0.91	0.87	0.91

above the theoretical line in most cases, especially in near-neutral conditions; nearly all the points were above the theoretical curve at DX. As mentioned above,  $T_*$  and  $L_{\text{Ob}}$  were obtained from EC, the inconsistencies in Fig. 4 were primarily caused by the difference in source area between EC and LAS measurements, uncertainties of some parameters (friction velocity, aerodynamic roughness length, etc.) (Zhang et al., 2010), and the degree of the surface homogeneity. Especially for MY site (with rolling terrain) and DX site (the EC system was located near the transmitter of LAS), the values were above the theoretical line.

### 3.2. Source areas of flux measurements

The source areas of EC and LAS were calculated for the MY, DX and GT sites in January and July (Fig. 5), which represented the

non-growing season and plant growing season. As depicted in Fig. 5, the source areas of the EC and LAS measurements at MY extended from the northeast to the southwest, with the main contribution area of EC at 400 m long and 250 m wide, although there were some differences between January and July due to the different wind direction; the LAS source area distributed along its path length, within a 1700 m long and 350 m wide area in both January and July. The underlying surface of the source areas of EC primarily consisted of orchards and bare soil/maize, and the LAS source area contained orchards, bare soil/maize, and residential areas. The EC was located at the transmitter side of the LAS at DX, and the source areas of EC and LAS had great changes in January and July, varying with the wind direction. The primary contributing source area of the EC measurements was within a 200 m radius of the observation point in January and localized within  $300 \text{ m} \times 200 \text{ m}$  (northwest-southeast) in July; the LAS source area at DX extended from the northeast to the southwest in both January and July, within a area of  $2400 \text{ m} \times 1200 \text{ m}$  in January, and  $2400 \text{ m} \times 900 \text{ m}$  in July. The source areas of EC at DX were covered with winter wheat/maize; however, the primary land cover was winter wheat/maize, vegetables, and fruit in the LAS source area. Though the source areas of EC and LAS at GT extended from the south to the north direction in both January and July, there were great changes in

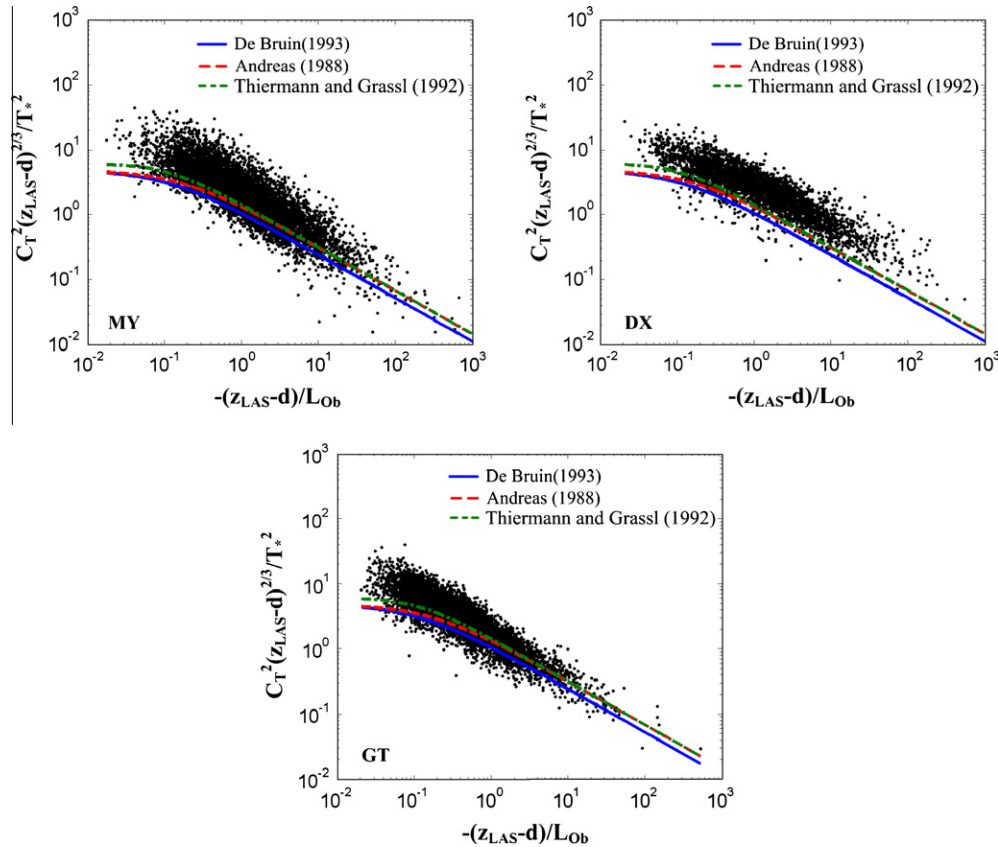


**Fig. 4.** Observed values of  $C_T^2(z_{LAS} - d)^{2/3}/T_*^2$  were plotted against  $(z_{LAS} - d)/L_{Ob}$  under unstable conditions for the years 2008–2010 at MY, DX and GT (the sensible heat flux was greater than  $50 \text{ W m}^{-2}$ ).

the scope of both the EC and LAS measurements. In January, the EC source area was in 1200 m long and 800 m wide, whereas it was 900 m long and 500 m wide in July; the source areas of the LAS measurements in January was larger than in July, however, distributed approximately 2700 m long and 700 m wide. The underlying surface within the source areas of EC and LAS measurements at GT was primarily winter wheat and bare soil in January and maize and cotton in July.

### 3.3. The characteristics of related environmental conditions

To analyze the variation in ET more clearly, it is necessary to quantitatively understand of the environmental factors affecting ET at each site. The characteristics of precipitation, air temperature, vapor pressure deficit (VPD), leaf area index (LAI), soil moisture and available energy ( $R_n - G_0$ ) from 2008 to 2010 are plotted in Fig. 6. LAI is the product of MODIS (MODIS15A2, 8-day composites), and soil moisture is the average moisture of 0–60 cm observations.

Over the study period, most of the annual precipitation was concentrated in the wet season, from June to September. The average annual precipitation was 589.20 mm, 446.38 mm, and 490.39 mm for MY, DX and GT, respectively in 2008–2010. The highest precipitation was in 2010 at MY and GT (640.50 mm and 577.60 mm), whereas it occurred in 2008 at DX (561.93 mm); the air temperature had consistent variation in the range of  $-10^\circ\text{C}$  to  $30^\circ\text{C}$  at the three sites; the maximum temperature occurred in July or August, the minimum was in December or January, and there was no obvious change between the three years. MY site was located in a mountainous area with relatively higher elevation (350 m vs. 20 and 30 m at DX and GT, respectively); thus, the air temperature was relative lower than at the other two sites. The

VPD showed clear seasonal variations, with higher values recorded during the growing seasons from May to June; the maximum value was greater than 2 Kpa (in 2009) at the three sites, and there was no obvious difference between the three sites. The LAI and soil moisture exhibited significant differences among the sites. The maximum values of LAI appeared in July at MY ( $3.2/2.4/2.9 \text{ m}^2 \text{ m}^{-2}$  in the year of 2008/2009/2010) and showed two peak values per year at DX and GT around one year, which were  $1.1/1.1/1.5$ ,  $1.1/1.0/1.1 \text{ m}^2 \text{ m}^{-2}$  in April or May and  $3.0/2.5/2.0$ ,  $4.2/2.5/2.1 \text{ m}^2 \text{ m}^{-2}$  in August in 2008/2009/2010, respectively. In the crop growing season, the average soil moisture remained at a high level (the volumetric water content was approximately 30%) at the three sites, and there was no obvious change among the years. Because of the irrigation of cropland at DX and GT, the soil moisture at those two sites was higher than at MY. The available energy reached the maximum during July to August (the average daily net radiation was approximately  $150 \text{ W m}^{-2}$ ). The available energy at MY was larger at the other two sites. There was also no obvious change in available energy among the three years.

### 3.4. Seasonal and interannual variations in evapotranspiration over the HRB

The seasonal and interannual variations in ET measured by EC and LAS at the three sites from 2008 to 2010 are presented in Fig. 7. ET measured by EC was corrected using the Bowen-ratio closure method proposed by Twine et al. (2000), and ET measured by LAS was obtained using the energy balance residual method (Eq. (6)).

The seasonal variation in ET measured by EC and LAS showed similar trends at the three sites (Fig. 7), and the ET variation was closely associated with the crop planting structure at each site,

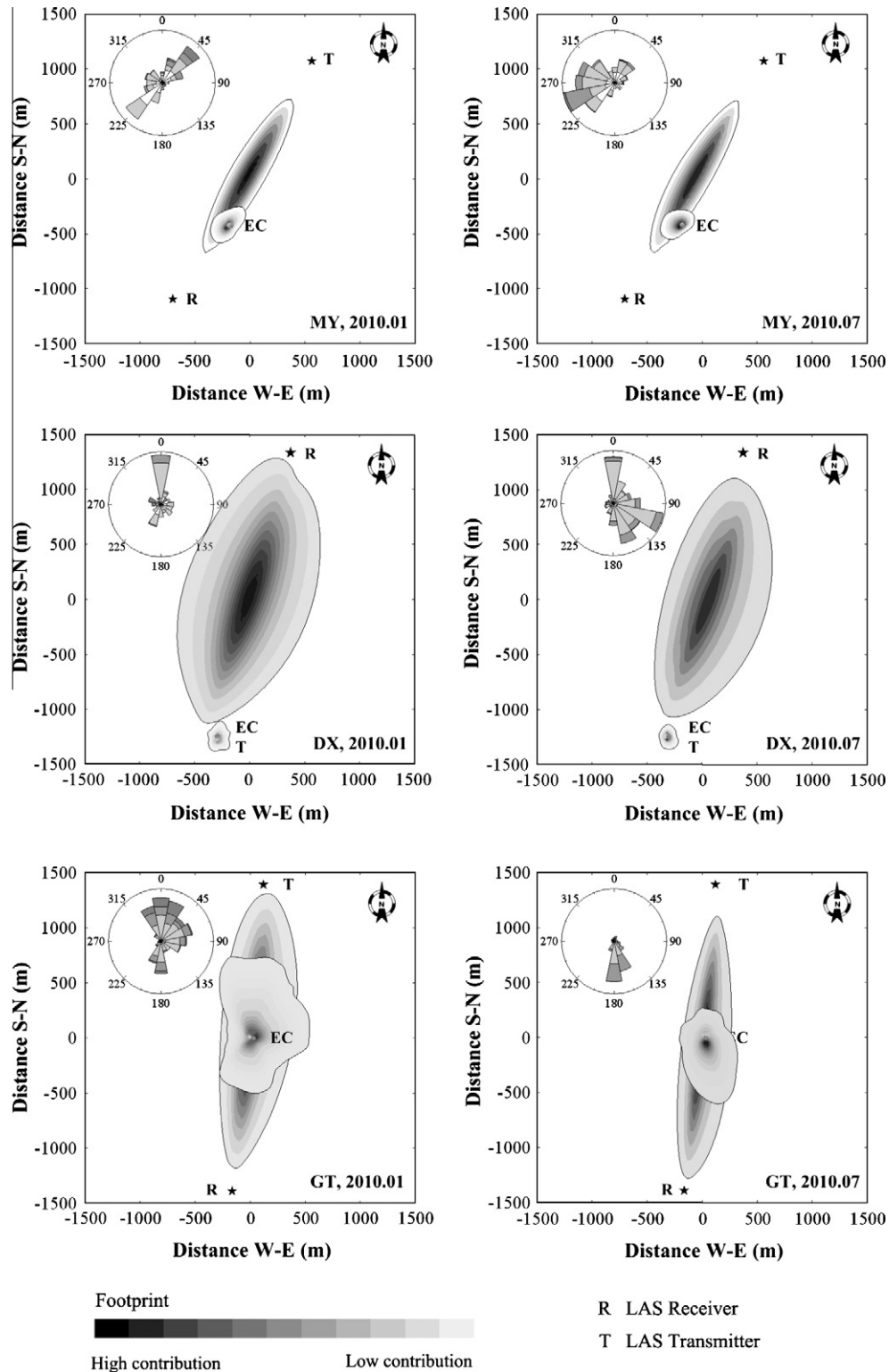
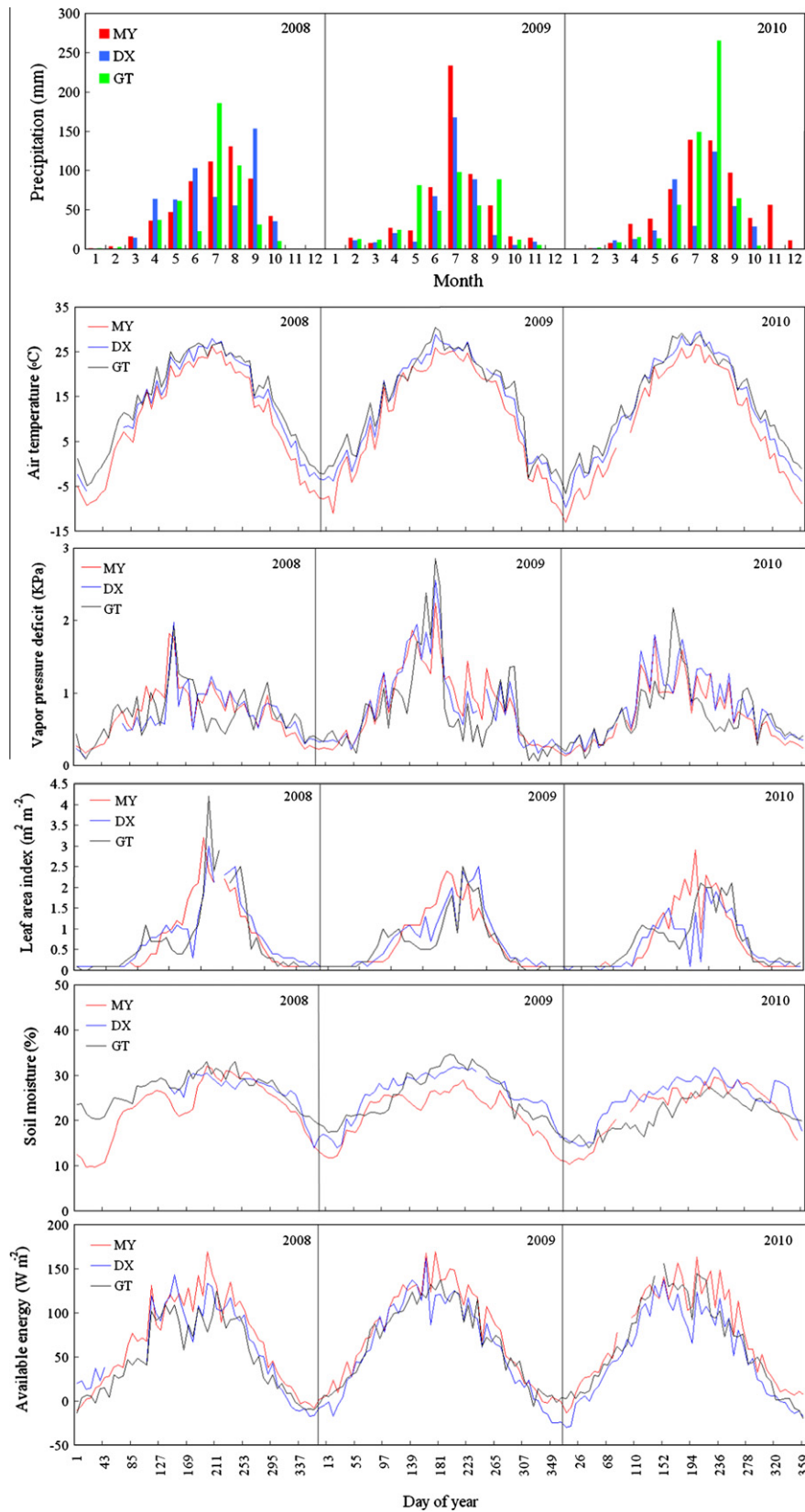


Fig. 5. Source areas of the EC and LAS measurements at the different sites (the source area of 50% contribution to the measured fluxes at MY, 80% at DX and GT).

where summer maize or orchard is planted at MY per annual, winter wheat is rotated with summer maize at DX and GT. Also, cotton was grown during the period of May to September at GT. ET exhibited a single peak at MY per year; the maximum ET measured by EC and LAS appeared in July in 2008 and 2009 and in August in 2010. At MY, the annual ET measured by EC was 582.07, 602.07, and 626.72 mm in 2008, 2009 and 2010, whereas the annual ET

measured by LAS was 448.67, 434.89, and 510.27 mm during those three years. The ET at DX and GT exhibited two peaks per year, appearing in May and August (it was July at GT in 2009 and 2010). The cumulative ET at DX was 650.30, 729.29, and 614.55 mm in 2008, 2009 and 2010 as measured by EC, and it was 531.46 and 450.61 mm in 2009 and 2010 as measured by LAS. The annual ET measured by EC at GT was 515.95, 645.74,





**Fig. 6.** The variation in precipitation, air temperature, vapor pressure deficit, leaf area index, soil moisture, and available energy from 2008 to 2010 (the precipitation is the monthly cumulative value, leaf area index is the product of MODIS (8 days average), the others variables were 7 days averages).

and 664.27 mm in 2008, 2009, and 2010 and the annual ET measured by LAS was 469.72, 524.17, and 559.21 mm, respectively. At MY, the year with the lowest precipitation also had the lowest

ET, which means that ET was primarily associated with precipitation, whereas in the irrigated fields at DX and GT, in addition to precipitation, ET was also connected with the amount of irrigation.

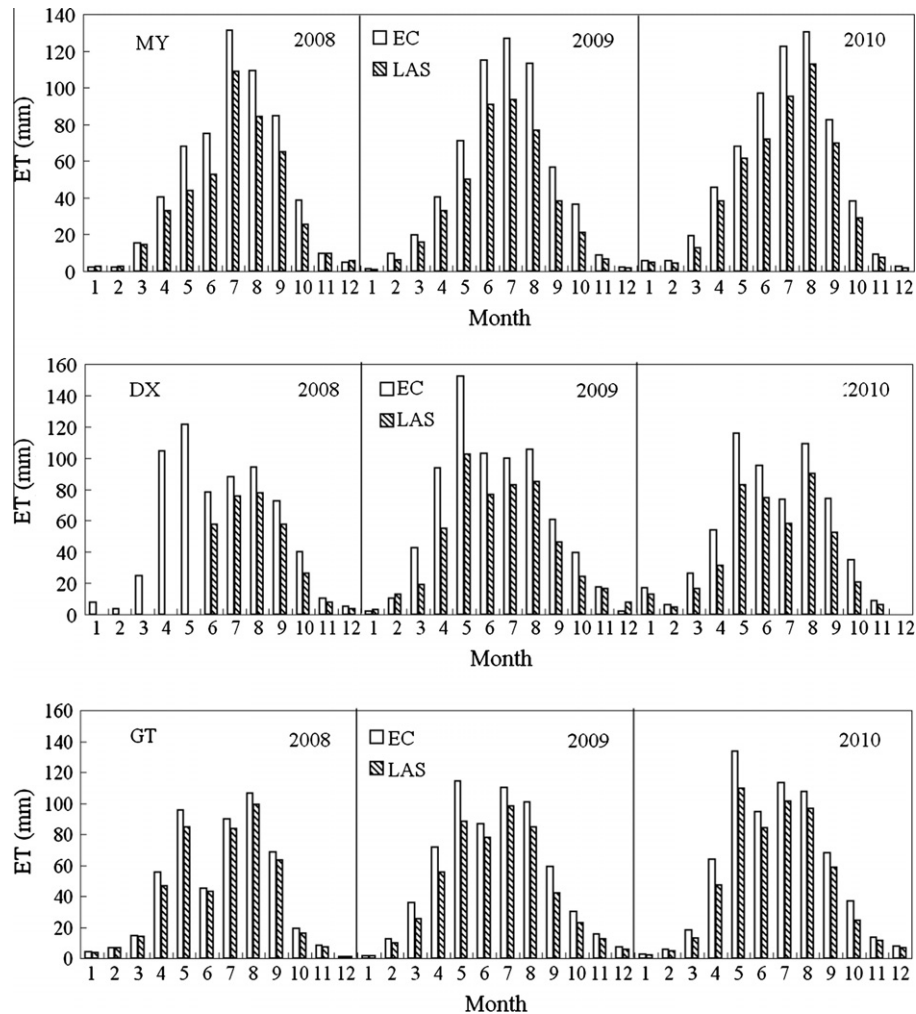


Fig. 7. The monthly ET variations measured by EC and LAS in 2008–2010 across the HRB.

The measured ET at the three sites was similar to the results obtained by Lei and Yang (2010), whose study area was the Weishan irrigation district in the HRB and whose cumulative ET values were 610, 595, and 554 mm measured by EC during the whole crop growing season (winter wheat and maize) in the years 2005 to 2008.

The comparisons of cumulative ET and precipitation are presented in Fig. 8, where the ET data were obtained from EC in 2009 at MY, DX and GT. Fig. 8 illustrated that the precipitation and ET were more or less in balance at MY, whereas ET was higher than precipitation at DX and GT. ET was very low before the Julian day of 50, the cumulative ET at that point being less than 10 mm. Afterwards, ET increased gradually, especially at DX and GT because of the winter wheat growth, irrigation and increasing air temperature. The ET was roughly equal to precipitation at MY in non-irrigated field, where the cumulative precipitation and ET were 564.50 mm and 602.07 mm, respectively. At DX, the cumulative precipitations, amount of irrigation, and ET in 2009 were 404.30, 337.80, and 729.29 mm; whereas they were 435.86 mm in precipitation, 181.75 mm in irrigation amount, and 645.74 mm in ET at GT. Overall, the revenues and expenditures of water resources at the three sites were roughly in equilibrium (see Section 3.5).

Fig. 7 indicates that the ET measured by LAS was smaller than the EC measurements at all sites during 2008–2010. To explain this phenomenon more clearly, the GT cropland site in the plain was

taken as an example. The flux contributions of different underlying surfaces calculated by the footprint model combining the land use/cover map were plotted in Fig. 9. The observing period was the whole winter wheat and maize growing season, from October 2009 to October 2010. The average sensible heat flux during different crop phenology period was also plotted. The various types of underlying surfaces contributing to the EC and LAS measurements had no significant differences during the growing season of winter wheat and maize; the flux contribution percentage of winter wheat/maize in the source area was 65–70%, the bare soil/cotton proportion was 22–30%, and other types (e.g., country road) were approximately 3–7%. Meanwhile, the sensible heat fluxes measured by EC and LAS exhibited a similar trend to the growth of crops; however, the observed values were different. That is to say, the flux contributions of various underlying surfaces were similar in the EC and LAS source areas (even the same contribution, such as the stem extension of winter wheat, harvesting of maize); however, differences in crop growing conditions in the field and soil moisture caused the sensible heat flux difference between EC and LAS measurements and also the ET difference.

Hoedjes et al. (2007) indicated that radiative surface temperatures obtained from thermal infrared satellite imagery can provide a good indication of the degree of heterogeneity within the experimental area and can be used to identify the differences between the EC and LAS measurements. In the present study, the surface temperatures from five Thematic Mapper (TM) images (27 Mar.

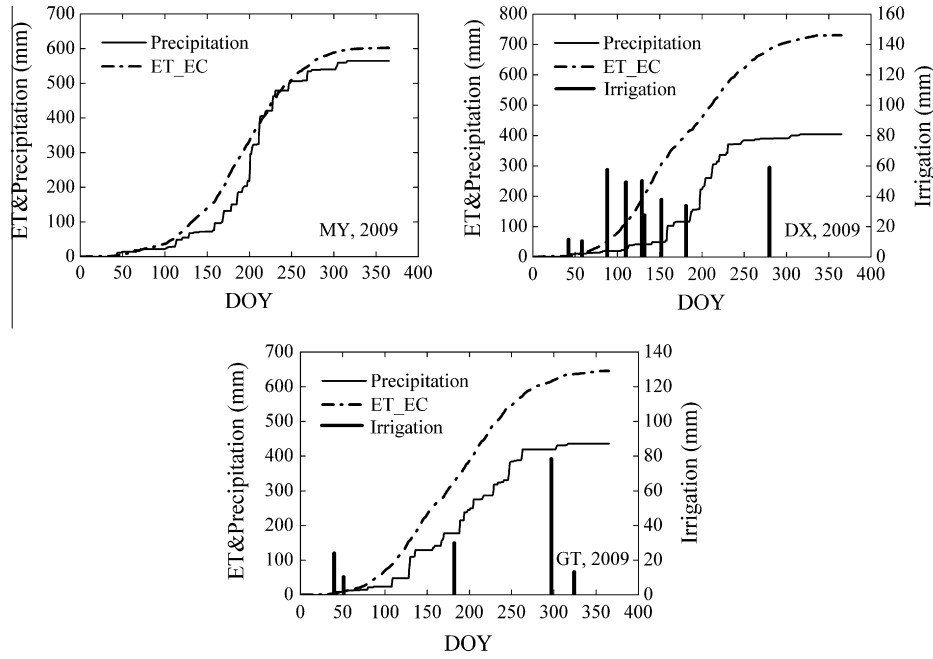


Fig. 8. The comparison of cumulative ET, precipitation, and irrigation in 2009 at the three sites over the HRB.

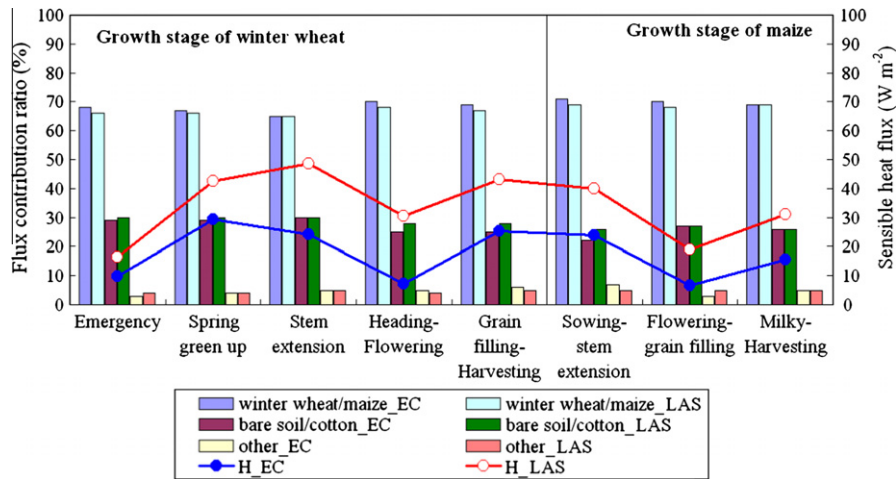


Fig. 9. The sensible heat flux and the flux contribution at different crop growing stages during 2009–2010.

and 14 May in 2008, 02 Apr., 05 Jun., 21 Jun. in 2010) with an overpass time of 10:45 BST were used to further analyze the reasons for the difference in sensible heat fluxes measured by EC and LAS. The sensible heat flux difference ( $\Delta H$ ), the absolute value of weight surface temperature difference in the LAS and EC source area ( $abs(\Delta T_s)$ ), and the EBR were listed in Table 3.  $\Delta T_s$  was defined as:

$$abs(\Delta T_s) = \left| \sum_{i=1}^m (FP_{LAS_i} \cdot T_{s_i}) / m - \sum_{j=1}^n (FP_{EC_j} \cdot T_{s_j}) / n \right| \quad (11)$$

where  $FP_{LAS_i}$  and  $FP_{EC_j}$  are the normalized footprints of 30-min LAS and EC measurements at grids  $i$  and  $j$  during the satellite passing time,  $T_{s_i}$  and  $T_{s_j}$  are the surface temperatures at grids  $i$  and  $j$ , and  $m$  and  $n$  are the numbers of grids within the LAS and EC source areas, respectively. The indicator  $abs(\Delta T_s)$  not only reflected the difference in soil moisture between the EC and LAS source areas, but also reflected the difference in source areas between the EC and LAS measurements (Hoedjes et al., 2007).

Table 3 showed that when the EBRs were the same on 27 March 2008, 14 May 2008, and 21 June 2010, the  $abs(\Delta T_s)$  was positively proportional to  $\Delta H$ , and when the  $abs(\Delta T_s)$  was similar on the days of 05 June and 21 June 2010,  $\Delta H$  was much smaller when the EBR was larger. That means that the  $abs(\Delta T_s)$  and EBR together influenced the difference between the EC and LAS measurements.

At MY, the difference between the EC and LAS measurements was large in the plant growing season (April–September), whereas the difference was smaller in the dormant season. This phenomenon was caused by the different underlying surfaces in the EC and LAS source areas. The primary underlying surfaces in the EC's source area were orchards and maize/bare soil, vs. orchards, maize/bare soil, and residential surfaces in the LAS source area. In the plant growing season, the ET measured by LAS was thus smaller than the EC observations; however, the different underlying surfaces had similar ET values in the dormant season, and therefore, the ET values measured by LAS and EC were close to each other. At DX, there were no overlapping areas between the EC and

**Table 3**

The sensible heat flux difference ( $\Delta H$ ), the absolute value of weight surface temperature difference in the LAS and EC source area ( $\text{abs}(\Delta T_s)$ ), and the EBR in the TM overpass time.

Date	$\Delta H$ ( $\text{W m}^{-2}$ )	$\text{Abs}(\Delta T_s)$ (K)	EBR
27 March 2008	107.15	0.90	0.64
14 May 2008	88.54	0.38	0.64
02 April 2010	16.42	0.27	0.86
05 June 2010	28.88	0.11	0.75
21 June 2010	82.50	0.13	0.64

LAS source areas, and their observed ET values had a large difference.

From the above analysis, it is clear that the differences in annual ET among the years and sites were primarily connected with difference in soil moisture (caused by differences in precipitation and irrigation) and crop growing conditions (differences in crop structures, crop varieties, and tillage practice, etc.). The heterogeneity of the EC and LAS source areas and the difference in source areas between the EC and LAS measurements caused the differences between the EC and LAS measurements (Liu et al., 2011). Additionally, this gap filling method of LAS (set  $H_{LAS} = 0$  when  $H_{LAS} < 0$ ) will result in higher values of daily mean  $H_{LAS}$  and thus ET derived from LAS is underestimated. This is an important reason why ET from LAS is lower than the one from EC. Notably, the ET value acquired from LAS was through the energy balance residual method; however, the instrument measurement scales of net radiation and surface soil heat flux do not match that of the LAS observations, leading to some uncertainties in the ET measured by LAS.

### 3.5. Comparison of ET measured by EC and LAS with other estimation methods

#### 3.5.1. Comparison of ET measured by EC with the field water balance method

This section compares the ET measured by EC with the estimate from the field water balance method. The field water balance method was based on the principle of conservation of mass:

$$ET = P + I + W - R - D - \Delta S \quad (12)$$

where  $P$  is precipitation,  $I$  is irrigation,  $W$  is the contribution from the ground water table,  $R$  is surface runoff,  $D$  is the deep drainage, and  $\Delta S$  is the change in water storage. The surface runoff  $R$  was neglected because the experimental site was flat. The contribution from the ground water table  $W$  was considered negligible, as the ground water table was over 28 m deep. The deep drainage  $D$  was neglected because the 60–100 cm soil moisture changed very little after precipitation at MY, DX and GT sites. The soil water balance Eq. (12) can therefore be simplified as:

$$ET = P + I - \Delta S \quad (13)$$

ET was calculated using Eq. (13), where irrigation was calculated using the observed soil moisture change before and after irrigation

(and validated with the field investigations by local farmers), and the change in water storage  $\Delta S$  was calculated using the soil moisture data at the beginning and ending of the year.

The ET measured by EC and the estimate of the field water balance method are roughly equal to each other (Table 4), with the mean relative error (MRE) was in the range from –10.28% to 9.71%, the root mean square error (RMSE) was in the range from 7.02 to 76.13 mm at the three sites during 2008–2010. The difference can be regarded as the uncertainties in the field water balance method (e.g.,  $W$ ,  $R$ ,  $D$  cannot be neglected), water supply from the groundwater by capillary action, the uncertainties of the EC measurements, and instrument errors in the field observations (e.g., errors of precipitation measurement, soil moisture measurement was not deep enough). In short, we considered the EC observations to be reliable.

#### 3.5.2. Comparison of the ET measured by LAS with MODIS ET products (MOD16 ET)

The MODIS Global Evapotranspiration Project (MOD16) is a part of NASA/EOS project to estimate global terrestrial ET from earth land surface by using satellite remote sensing data. The MOD16 global ET datasets are regular  $1 \text{ km}^2$  land surface ET data sets for the 109.03 million  $\text{km}^2$  of global vegetated land areas at 8-day, monthly and annual intervals, which are blank in the regions of water bodies, wetlands, urban and built-up areas. The MOD16 ET datasets are estimated using Mu et al.'s improved ET algorithm (2011) based on MODIS and global meteorology data, which was developed from the Penman–Monteith equation. The monthly MOD16 ET products for 2008–2010 over the HRB were used in this study (<http://www.nts.gov.cn/project/mod16>).

Fig. 10 is a comparison of monthly ET values measured by LAS and MOD16 ET values at MY, DX and GT from 2008 to 2010, with the statistics shown in Table 5. The validation pixels were selected with the help of the footprint model. Specifically, the images of the MOD16 monthly ET were overlapped with the footprint-weighted images of LAS, and pixels within the source area were taken as the validation pixels. Then, the footprint weights within each pixel were summed, and the weighted average of the remote sensing values could be computed (Jia et al., 2012).

Overall, the MRE of monthly ET measured by LAS and MOD 16 ET values was in the range from –14.52% to 25.16%, the RMSE was in the range from 0.14 to 112.41 mm, correlation coefficient ( $R$ ) was in the range from 0.76 to 0.97 at the three sites. The smallest difference between the ET measured by LAS and the MOD16 ET was found at MY and the largest difference was at GT site. These differences were caused by the following factors: (1) MOD16 ET was produced at a global scale, and the variation in the spatial pattern in the MOD16 ET distribution was relatively smoothed, which may be affected by the input datasets, such as  $1^\circ \times 1.25^\circ$  meteorological data and  $0.05^\circ$  albedo data, etc. (2) MOD16 ET cannot reflect the characteristics of the variation in typical double-cropping system across the HRB. The observed ET had two peaks per year with

**Table 4**

The comparison of ET measured by EC with the field water balance estimation from 2008 to 2010 at the three sites over the HRB at annual scale.

Site	Year	ET_EC (mm)	Precipitation (mm)	Irrigation (mm)	ET_Water budget (mm)	MRE (%)	RMSE (mm)
MY	2008	582.07	562.60	0	559.17	4.10	22.90
	2009	602.07	564.50	0	548.80	9.71	53.27
	2010	626.72	640.50	0	609.80	2.77	16.92
DX	2008	650.30	561.93	176.80	658.47	–1.24	8.17
	2009	729.29	404.30	337.80	712.00	2.43	17.29
	2010	614.55	372.90	305.80	672.60	–8.63	58.05
GT	2008	515.95	457.70	86.04	508.93	1.38	7.02
	2009	645.74	435.86	181.75	601.31	7.39	44.43
	2010	664.27	577.60	179.55	740.40	–10.28	76.13



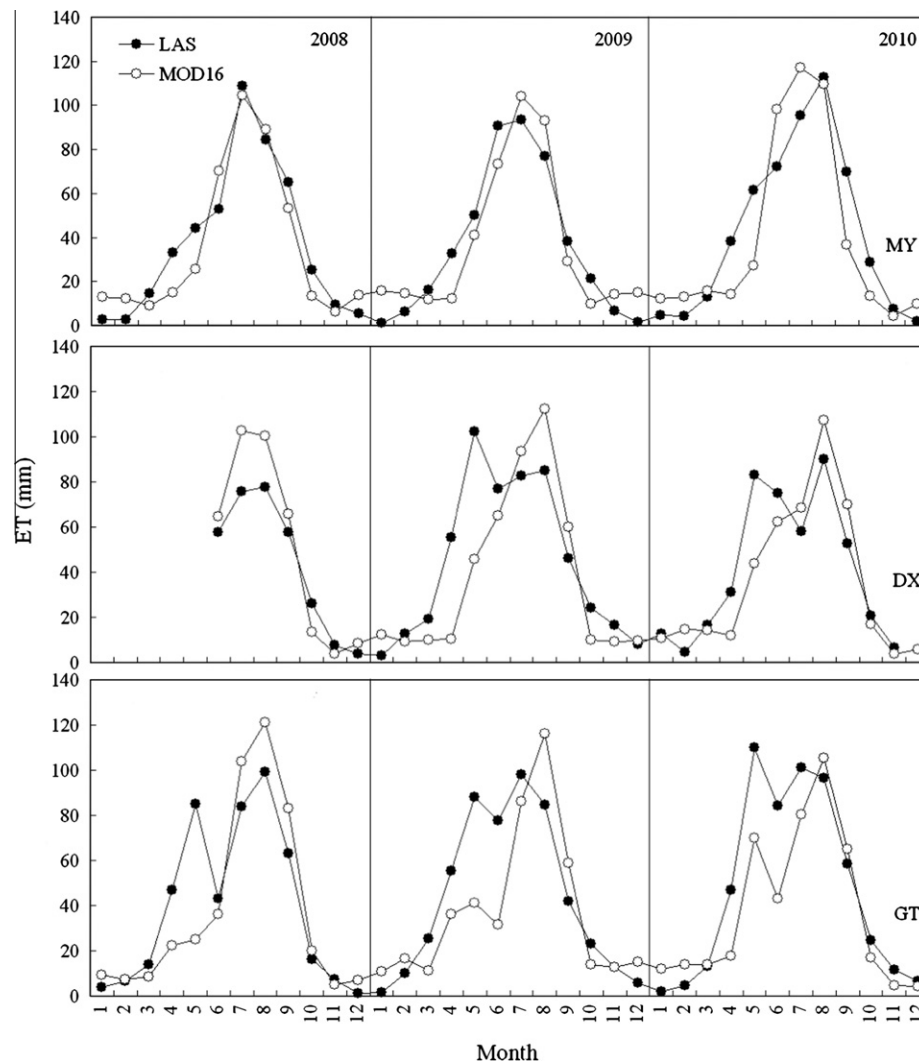


Fig. 10. Comparison of MOD 16 ET with LAS observations during 2008–2010 at the three sites over the HRB.

Table 5

Comparison of ET measured by LAS with MOD16 ET at annual scale.

Site	Year	MRE (%)	RMSE (mm)	R
MY	2008	5.41	23.01	0.94
	2009	0.03	0.14	0.92
	2010	7.98	37.73	0.86
DX	2008	−14.52	52.08	0.97
	2009	17.47	76.58	0.77
	2010	6.66	26.25	0.85
GT	2008	4.73	21.22	0.80
	2009	16.52	74.34	0.76
	2010	25.16	112.41	0.89

the double-cropping systems at GT and DX; however, most of the MOD16 ET had only one peak. The largest error between MOD16 ET and LAS observations was appeared in May (the peak growth period of winter wheat) during 2008–2010 (Fig. 10). In addition, the possible reasons for the difference included field observation errors (instrument bias, gap filling data, etc.), error resulting from MODIS pixel drifting, etc. Overall, the LAS measurements can reflect the spatial and temporal variation in ET, and the LAS observations are reliable.

### 3.5.3. Comparison of ET by EC and LAS with measurements by previous researchers

Given the unique location of the HRB (including the mega cities of Beijing, Tianjin, etc. and a major food production area of China) and the fact of water resource shortages, many papers have been published about the ET in the basin. Fig. 11 shows the ET results in the whole crop (winter wheat/maize) growing season measured by lysimeter, EC and LAS by different researchers during 1995–2010 (Lei and Yang, 2010; Liu et al., 2002; Liu and Luo, 2010), which also shows the DX and GT results. The ET decreased slightly from 1995 to 2010 (Fig. 11), which was consistent with the studies by Liu et al. (2005), whose paper showed that the water requirements of the main crop decreased during 1950–2000 across the HRB. To sum up, the reasons for the above phenomena were (i) precipitation exhibited a decreasing trend across the HRB (Wang et al., 2011); (ii) the improvement of irrigation technology (Wu et al., 2010). Although the irrigation area was increased year by year (New China Agriculture Compendium of Statistics 1949–2008), the actual quantity of irrigation water trended downward. Water-saving irrigation techniques have been popularized in recent years, and the new ideas and technologies in agricultural water management have been implemented (Miao et al., 2010), which are also causing a decrease in the amount of irrigation;

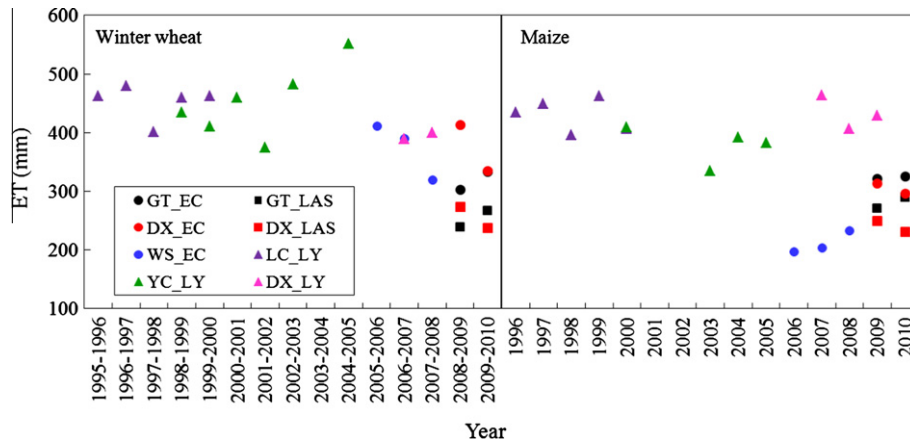


**Fig. 11.** Comparison of ET between different years and instruments over the HRB (LC, Luancheng (37°53', 114°41', Liu et al., 2002); YC, Yucheng (37°50', 114°40', Liu and Luo, 2010); WS, Weishan irrigation area (36°39', 116°03', Lei and Yang, 2010)).

and (iii) the meteorological conditions related to ET differ among the studied years and sites.

#### 4. Conclusions

In this study, the source areas of EC and LAS were determined at each site, analyzed the seasonal and interannual variation in ET based on two observations scales (EC and LAS) after rigorous data processing and quality control in the HRB, and gave a quantitatively analysis of ET for the primary underlying surfaces of the HRB. Comparisons were also made between the ET values measured by EC and LAS and the field water balance method calculation and the MOD16 ET product, respectively.

Data quality at each site can meet the long-term flux variations analysis. The quality of the EC data is consistent with that of Fluxnet data; the average available data percentage was 69% at MY, 57% at DX, and 84% at GT in the years 2008–2010. The EBR of EC is in the range of 0.78–0.91 at the three sites. The LAS data were consistent with the theoretical line at GT, whereas they were a little above the theoretical line at MY and DX, but followed the same trend. Considering the unexpected surface heterogeneity and the instrument's inherent characteristics and their setting positions, the LAS data were reliable.

The annual ET measured by EC was in the range of 510–730 mm during 2008 to 2010 across the basin, with 582.07, 602.07, and 626.72 mm at MY, 650.30; 729.29, and 614.55 mm at DX; and 515.95, 645.74, and 664.27 mm at GT. The LAS measurements were between 430–560 mm, with 448.67, 434.89, and 510.27 mm at MY; 531.46, and 450.61 mm in 2009 and 2010 at DX; and 469.72, 524.17, and 559.21 mm at GT. The differences in ET among the years and sites were primarily connected with the difference in soil moisture (caused by difference in precipitation and irrigation) and crop growing conditions (differences in crop structures, crop varieties, and tillage practice, etc.). The heterogeneity of the underlying surfaces in the EC and LAS source areas and the difference in their source areas are the primary reasons causing the difference in measurements between EC and LAS.

The ET values measured by EC and LAS were compared with the field water balance method calculation and MOD16 ET, respectively. The average difference between the EC measurements and field water balance method calculations was 0.85% and 33.80 mm for MRE and RMSE, respectively, whereas the average difference between the LAS measurements and MOD 16 ET was 7.72% and 47.08 mm for MRE and RMSE, respectively, from 2008 to 2010 at the three sites. We also compared our data with the results of studies by previous researchers in these sites in the HRB,

finding that the ET appears to have decreased over the past 15 years, especially after 2005.

#### Acknowledgments

This work was funded by the National Natural Science Foundation of China (30911130504 and 40971194), the Fundamental Research Funds for the Central Universities and Global Environment Facility (GEF) Project (TF053183). The lysimeter data at DX site are provided by Prof. Y. Liu from China Institute of Water Resources and Hydropower Research.

#### References

- Alavi, N., Warland, J.S., Berg, A.A., 2006. Filling gaps in evapotranspiration measurements for water budget studies: evaluation of a Kalman filtering approach. *Agric. For. Meteorol.* 141, 57–66.
- Andreas, E.L., 1988. Estimating  $C_n^2$  over snow and sea ice from meteorological data. *J. Opt. Soc. Am.* 5, 481–495.
- Aubinet, M., Grelle, A., Ibrom, A., Rannik, U., Moncrieff, J., Foken, T., Kowalski, A.S., Martin, P.H., Berbigier, P., Bernhofer, Ch., Clement, R., Elbers, J., Granier, A., Grünwald, T., Morgenstern, K., Pilegaard, K., Rebmann, C., Snijders, W., Valentini, R., Vesala, T., 2000. Estimates of the annual net carbon and water exchange of European forests: the EUROFLUX methodology. *Adv. Ecol. Res.* 30, 113–174.
- Baldocchi, D.D., 2003. Assessing the eddy covariance technique for evaluating carbon dioxide exchange rates of ecosystems: past, present and future. *Global Change Biol.* 9, 479–492.
- Beyrich, F., De bruin, H.A.R., Meijninger, W.M.L., 2002. Results from one-year continuous operation of a large aperture scintillometer over a heterogeneous land surface. *Bound.-Layer Meteorol.* 105, 85–97.
- Blanken, P.D., Black, T.A., Neumann, H.H., Hartog, C.D., Yang, P.C., Nesic, Z., Staebler, R., Chen, W., Novak, M.D., 1998. Turbulence flux measurements above and below the overstory of a boreal aspen forest. *Boun.-Layer Meteorol.* 89, 109–140.
- De Bruin, H.A.R., Kohsiek, W., Hurk, B.J.J.M.v.d., 1993. A verification of some methods to determine the fluxes of momentum, sensible heat and water vapor using standard deviation and structure parameter of scalar meteorological quantities. *Bound.-Layer Meteorol.* 63, 231–257.
- Ezzahar, J., Chehbouni, A., Hoedjes, J.C.B., Er-Raki, S., Chehbouni, Ah., Boulet, G., Bonnefond, J.M., De Bruin, H.A.R., 2007. The use of the scintillation technique for monitoring seasonal water consumption of olive orchards in a semi-arid region. *Agric. Water Manage.* 89, 173–184.
- Falge, E., Baldocchi, D.D., Olson, R., Anthoni, P., Aubinet, M., Bernhofer, C., Burba, G., Ceulemans, R., Clement, R., Dolman, H., Granier, A., Gross, P., Grünwald, T., Hollinger, D., Jensen, N.O., Katul, G., Keronen, P., Kowalski, A., Lai, C.T., Law, B.E., Meyers, T., Moncrieff, J., Moors, E., Munger, J.W., Pilegaard, K., Rannik, U., Rebmann, A., Suyker, C., Tenhunen, J., Tu, K., Verma, S., Vesala, T., Wilson, K., Wofsy, S., 2001. Gap filling strategies for defensible annual sums of net ecosystem exchange. *Agric. For. Meteorol.* 107, 43–69.
- Finnigan, J., 2004. The footprint concept in complex terrain. *Agric. For. Meteorol.* 127, 117–129.
- Foken, T., Wichura, B., 1996. Tools for quality assessment of surface-based flux measurements. *Agric. For. Meteorol.* 78, 83–105.
- Foken, T., Göckede, M., Mauder, M., Mahrt, L., Amiro, B., Munger, W., 2004. Post-field data quality control. In: Lee, X., Massman, M., Law, B. (Eds.), *Handbook of*

- Micrometeorology. A Guide for Surface Flux Measurement and Analysis. Kluwer Academic, Boston, pp. 181–208.
- Foken, T., Mauder, M., Liebethal, C., Wimmer, F., Beyrich, F., Leps, J.P., Raasch, S., De Bruin, H.A.R., Meijninger, W.M.L., Bange, J., 2010. Energy balance closure for the LITFASS-2003 experiment. *Theor. Appl. Climatol.* 101, 149–160.
- Foken, T., Aubinet, M., Finnigan, J.J., Leclerc, M.Y., Mauder, M., Pawu, K.T., 2011. Results of a panel discussion about the energy balance closure correction for trace gases. *Bull. Am. Meteorol. Soc.* 92, ES13–ES18.
- Hammerle, A., Haslwanter, A., Schmitt, M., Bahn, M., Tappeiner, U., Cernusca, A., Wohlfahrt, G., 2007. Eddy covariance measurements of carbon dioxide, latent and sensible energy fluxes above a meadow and a mountain slope. *Bound.-Layer Meteorol.* 122, 397–416.
- Hartogensis, O.K., Watts, C.J., Rodriguez, J.C., De Bruin, H.A.R., 2003. Derivation of an effective height for scintillometers: La Poza Experiment in Northwest Mexico. *J. Hydrometeorol.* 4, 915–928.
- Hemakumara, H.M., Chandrapala, L., Moene, A.F., 2003. Evapotranspiration fluxes over mixed vegetation areas measured from large aperture scintillometer. *Agric. Water Manage.* 58, 109–122.
- Hoedjes, J.C.B., Chehbouni, A., Ezzahar, J., Escadafal, R., De Bruin, H.A.R., 2007. Comparison of large aperture scintillometer and eddy covariance measurements: can thermal infrared data be used to capture footprint-induced differences? *J. Hydrometeorol.* 8, 144–159.
- Jia, Z.Z., Liu, S.M., Xu, Z.W., Chen, Y.J., Zhu, M.J., 2012. Validation of remotely sensed evapotranspiration over the Hai River Basin, China. *J. Geophys. Res.* 117, D13113. <http://dx.doi.org/10.1029/2011JD017037>.
- Kleissl, J., Hong, S.H., Hendrickx, J.M.H., 2009. New Mexico scintillometer network: supporting remote sensing and hydrologic and meteorological models. *Bull. Am. Meteorol. Soc.* 90, 207–218.
- Kormann, R., Meixner, F.X., 2001. An analytic footprint model for neutral stratification. *Bound.-Layer Meteorol.* 99, 207–224.
- Lei, H.M., Yang, D.W., 2010. Interannual and seasonal variability in evapotranspiration and energy partitioning over an irrigated cropland in the North China Plain. *Agric. For. Meteorol.* 150, 581–589.
- Liu, Y.J., Luo, Y., 2010. A consolidated evaluation of the FAO-56 dual crop coefficient approach using the lysimeter data in the North China Plain. *Agric. Water Manage.* 97, 31–40.
- Liu, C.M., Yu, J., Kendy, E., 2001. Groundwater exploitation and its impacts on the environment in the North China. *Water Int.* 26, 265–272.
- Liu, C.M., Zhang, X.Y., Zhang, Y.Q., 2002. Determination of daily evaporation and evapotranspiration of winter wheat and maize by large-scale weighting lysimeter and micro-lysimeter. *Agric. For. Meteorol.* 111, 109–120.
- Liu, X.Y., Li, Y.Z., Hao, W.P., 2005. Trend and causes of water requirement of main crops in North China in recent 50 years. *Trans. CSAE* 20, 155–159 (in Chinese, abstract in English).
- Liu, S.M., Xu, Z.W., Wang, W.Z., Jia, Z.Z., Zhu, M.J., Wang, J.M., 2011. A comparison of eddy-covariance and large aperture scintillometer measurements with respect to the energy balance closure problem. *Hydrol. Earth Syst. Sci.* 15, 1291–1306.
- Mauder, M., Oncley, S.P., Vogt, R., Weidinger, T., Ribeiro, L., Bernhofer, C., Foken, T., Kohsiek, W., De Bruin, H.A.R., Liu, H.P., 2007a. The energy balance experiment EBEX-2000. Part II: Intercomparison of eddy-covariance sensors and post-field data processing methods. *Bound.-Layer Meteorol.* 123, 29–54.
- Mauder, M., Desjardins, R.L., MacPherson, I., 2007b. Scale analysis of airborne flux measurements over heterogeneous terrain in a boreal ecosystem. *J. Geophys. Res.* 112, D13112. <http://dx.doi.org/10.1029/2006JD008133>.
- Meijninger, W.M.L., Green, A.E., Hartogensis, O.K., Kohsiek, W., Hoedjes, C.B., Zuurbier, R.M., De Bruin, H.A.R., 2002a. Determination of area-averaged water vapour fluxes with large aperture and radio wave scintillometers over a heterogeneous surface-Flevoland field experiment. *Bound.-Layer Meteorol.* 105, 63–83.
- Meijninger, W.M.L., Hartogensis, O.K., Kohsiek, W., Hoedjes, J.C.B., Zuurbier, R.M., De Bruin, H.A.R., 2002b. Determination of the area-averaged sensible heat flux with a large aperture scintillometer over a heterogeneous surface-Flevoland field experiment. *Bound.-Layer Meteorol.* 105, 37–62.
- Miao, H.Y., Li, J.S., Zhao, L.H., Gu, Z.B., 2010. Characteristics of integrated water and environment plan in the Haihe River Basin. *South North Water Transf. Water Sci. Technol.* 8, 110–112 (in Chinese, abstract in English).
- Moene, A.F., Beyrich, F., Hartogensis, O.K., 2009. Developments in scintillometry. *Bull. Am. Meteorol. Soc.* 90, 694–698.
- Mu, Q., Zhao, M., Running, S.W., 2011. Improvements to a MODIS global terrestrial evapotranspiration algorithm. *Rem. Sens. Environ.* 15, 1781–1800.
- Ochs, G.R., Wilson, J.J., 1993. A Second-generation Large Aperture Scintillometer, NOAA Tech. Memor. ERL ETL-232. NOAA Environmental Research Laboratories, Boulder, CO, USA, 24pp.
- Oncley, S.P., Foken, T., Vogt, R., Kohsiek, W., De Bruin, H.A.R., Bernhofer, C., Christen, A., Gersel, E.V., Grantz, D., Feigenwinter, C., Lehner, I., Liebethal, C., Liu, H.P., Mauder, M., Pitacco, A., Ribeiro, L., Weidinger, T., 2007. The energy balance experiment EBEX-2000. Part I: overview and energy balance. *Bound.-Layer Meteorol.* 123, 1–28.
- Paulson, C.A., 1970. The mathematical representation of wind speed and temperature profiles in the unstable atmospheric surface layer. *J. Appl. Meteorol.* 9, 857–861.
- Rivas, R., Caselles, V., 2004. A simplified equation to estimate spatial reference evaporation from remote sensing-based surface temperature and local meteorological data. *Rem. Sens. Environ.* 93, 68–76.
- Schüttemeyer, D., Moene, A.F., Holtslag, A.A.M., De Bruin, H.A.R., De Giesen, N.A., 2006. Surface fluxes and characteristics of drying semi-arid terrain in west Africa. *Bound.-Layer Meteorol.* 118, 583–612.
- Suyker, A.E., Verma, S.B., 2009. Evapotranspiration of irrigated and rainfed maize-soybean cropping systems. *Agric. For. Meteorol.* 149, 443–452.
- Thiermann, V., Grassl, H., 1992. The measurement of turbulent surface layer fluxes by use of bichromatic scintillation. *Bound.-Layer Meteorol.* 58, 367–389.
- Twine, T.E., Kustas, W.P., Norman, J.M., Cook, D.R., Houser, P.R., Meyers, T.P., Prueger, J.H., Starks, P.J., Wesely, M.L., 2000. Correcting eddy-covariance flux underestimates over grassland. *Agric. For. Meteorol.* 103, 279–300.
- Von Randow, C., Kruit, B., Holtslag, A.A.M., De Oliveira, A.B.L., 2008. Exploring eddy-covariance and large-aperture scintillometer measurements in an Amazonian rain forest. *Agric. For. Meteorol.* 148, 680–690.
- Wang, T., Ochs, G., Clifford, S., 1978. Saturation-resistant optical scintillometer to measure Cn2. *J. Opt. Soc. Am.* 68, 334–338.
- Wang, Z.G., Luo, Y.Z., Liu, C.M., Xia, J., Zhang, M.H., 2011. Spatial and temporal variations of precipitation in Haihe River Basin, China: six decades of measurements. *Hydrol. Process.* 25, 2916–2923.
- Webb, E.K., 1970. Profile relationships: The log-linear range and extension to strong stability. *Q. J. Roy. Meteorol. Soc.* 96, 67–90.
- Wesely, M.L., 1976. The combined effect of temperature and humidity fluctuations on refractive index. *J. Appl. Meteorol.* 15, 43–49.
- Wever, L.A., Flanagan, L.B., Carlson, P.J., 2002. Seasonal and interannual variation in evapotranspiration, energy balance and surface conductance in a northern temperate grassland. *Agric. For. Meteorol.* 112, 31–49.
- Wilson, K.B., Baldocchi, D.D., 2000. Seasonal and interannual variability of energy fluxes over a broadleaved temperate deciduous forest in North America. *Agric. For. Meteorol.* 100, 1–18.
- Wilson, K.B., Goldstein, A., Falg, E., Aubinet, M., Baldocchi, D., Berbigier, P., Bernhofer, C., Ceulemans, R., Dolman, H., Field, C., Grelle, A., Ibrom, A., Law, B.E., Kowalski, A., Meyers, T., Moncrieff, J., Monson, R., Oechel, W., Tenhunen, J., Valentini, R., Verma, S., 2002. Energy balance closure at FLUXNET sites. *Agric. For. Meteorol.* 113, 223–243.
- Wu, P., Jin, J.M., Zhao, X.N., 2010. Impact of climate change and irrigation technology advancement on agricultural water use in China. *Clim. Change* 100, 797–805.
- Xia, J., Feng, H., Zhan, C., Niu, C., 2006. Determination of a reasonable percentage for ecological water-use in the Hai River Basin, China. *Pedosphere* 16, 33–42.
- Yang, K., Wang, J.M., 2008. A temperature prediction-correction method for estimating surface soil heat flux from soil temperature and moisture data. *Sci. China Ser. D* 51, 721–729.
- Yang, K., Koike, T., Yang, D., 2003. Surface flux parameterization in the Tibetan Plateau. *Bound.-Layer Meteorol.* 116, 245–262.
- Zhang, X.D., Jia, X.H., Yang, J.Y., Hu, L.B., 2010. Evaluation of MOST functions and roughness length parameterization on sensible heat flux measured by large aperture scintillometer over a corn field. *Agric. For. Meteorol.* 150, 1182–1191.